

COTODE: Continuous Trajectory neural Ordinary Differential Equations for modelling event sequences

Ilya Kuleshov
i.kuleshov@skoltech.ru
Skolkovo Institute of Science and
Technology
Moscow, Russia

Galina Boeva
Skolkovo Institute of Science and
Technology
Moscow, Russia

Vladislav Zhuzhel
Skolkovo Institute of Science and
Technology
Moscow, Russia

Evgenia Romanenkova
Skolkovo Institute of Science and
Technology
Moscow, Russia

Evgeni Vorsin
Innotech
Moscow, Russia

Alexey Zaytsev
Skolkovo Institute of Science and
Technology
Moscow, Russia

ABSTRACT

Observation of the underlying actors that generate event sequences reveals that they often evolve continuously. Most modern methods, however, tend to model such processes through at most piecewise-continuous trajectories. To address this, we adopt a way of viewing events not as standalone phenomena but instead as observations of a Gaussian Process, which in turn governs the actor's dynamics. We propose integrating these obtained dynamics, resulting in a continuous-trajectory modification of the widely successful Neural ODE model. Through Gaussian Process theory, we were able to evaluate the uncertainty in an actor's representation, which arises from not observing them between events. This estimate led us to develop a novel, theoretically backed negative feedback mechanism. Empirical studies indicate that our model with Gaussian process interpolation and negative feedback achieves state-of-the-art performance, with improvements up to 20% AUROC against similar architectures.

CCS CONCEPTS

• **Computing methodologies** → **Discrete-event simulation**; *Neural networks; Gaussian processes; Uncertainty quantification.*

KEYWORDS

Event Sequences, Deep Learning, Neural ODE, Gaussian Processes

1 INTRODUCTION

Sequences of events are integral to numerous fields of modern life. Examples of such data include bank transactions [4], patients' medical histories [20], various sales datasets [9], earthquake records [29], and more. One of its most critical characteristics is an uneven structure, which often necessitates complex modifications to the processing algorithm.

There are many existing methods for analysing event sequences. Traditional approaches model hidden data dynamics as a probabilistic process with certain constraints, e.g., Poisson [18] or Hawkes processes [16]. More advanced methods propose applying recurrent neural networks [14, 25] or transformers, often in combination with point processes [48]. Alternatively, recent research explores the use of ordinary differential equations (ODE) to process sequential data [10, 19, 21].

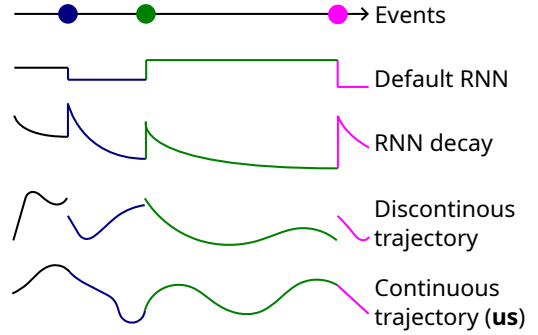


Figure 1: We propose to model the actor's latent representation continuously (see the bottom Continuous trajectory curve). Previously used approaches employ discontinuous trajectories: we demonstrate that this is empirically suboptimal for certain types of event sequences. Our approach also allows for an in-depth theoretical analysis.

ODEs are an old-but-gold approach, offering an intuitive way to handle time series and generate complex, informative trajectories, modelling the evolution of an actor's state. They are widely used in control theory and have been gaining popularity in modern sequence analysis. These models also allow one to adjust their *virtual depth*, i.e., how much they may influence the final hidden state. This is achieved by changing the tolerance parameters or step size of the solver, which in turn affects the number of evaluations. Evidently, conventional models lack this property. The first papers that apply Neural ODEs to event sequences employ a discontinuous hidden trajectory [19, 31]. Such jumps in trajectories are demonstrated to be detrimental to model quality by the authors of [21]. Instead, they reconstruct the inter-event path through interpolation and continuously feed this into the neural network-defined dynamics, thereby avoiding the need to disrupt the hidden trajectory. They argue that if the underlying process evolves continuously, the model should also do so. However, this method is only applicable to observations of a continuous process. This is not the case for event sequences.

We propose a new Neural ODE-based model that generates a continuous hidden trajectory, unlike other event sequence approaches. Our approach achieves continuity by defining the influence of

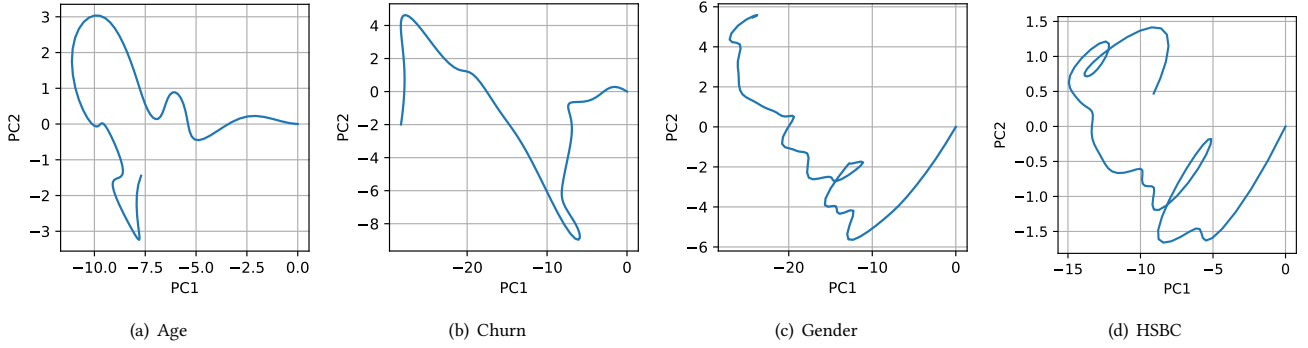


Figure 2: The generated continuous latent trajectories for four considered transactional datasets. We show the dynamics for the first two principal components (PC1 and PC2). The proposed COTODE model can produce complex paths that reflect the peculiarities of diverse datasets.

events in the space between them, and then using this influence to guide the hidden state without interruptions. This technique is particularly effective for systems where events cause gradual changes rather than sudden shocks. We demonstrate that the novel method achieves superior quality on downstream problems, indicating a more accurate simulation of the underlying process. Our contributions are as follows:

- A method to model the hidden trajectory built on Gaussian process (GP) regression. We interpolate event embeddings via GP and transform the resulting signal through a Neural ODE-like model, which allows us to produce a continuous hidden path.
- An analytical measure of the error in the integral representation, which arises from the lack of information about the client between events. We conclude that the raw ODE-based method is seriously flawed, with the error growing linearly with time.
- A procedure that addresses this issue in theory and practice, by introducing negative feedback into the ODE’s dynamics with an elegant implementation inspired by the GRU architecture. Our COTODE method is the combination of this procedure with GP-based interpolation of the input data.
- A diverse experimental study that includes retail, transactions, and wearable tracking systems and a comparison with state-of-the-art approaches based on RNNs or ODEs. These experiments demonstrate the broad applicability of our novel COTODE model, showing superior results across all the considered long-sequence datasets.
- Also, an ablation study that indicates that both the GP interpolation and the negative feedback are crucial for the success of the model.

2 RELATED WORKS

The study of event sequences has a long history, with roots in Temporal Point Processes (TPP) [16, 27]. Recently, this field has undergone significant changes due to the rapid development of Neural Network (NN) approaches. Below, we present a brief overview of relevant papers which inspired our research. The review starts

by examining the leading works on this subject. Next, we analyse prior studies that applied Neural ODEs to event sequences. Here, to emphasise our paper’s focus, we note the form of the hidden trajectory for each relevant ODE paper. The final part addresses the error estimates for Gaussian process regression, essential to our theoretical results.

Neural network approaches. There is a plethora of research on applying deep-learning methods directly to event sequences without fine-tuning them to the specifics of this field. They are primarily based on recurrent neural networks (RNNs) [1, 3, 4], although there are a few methods which utilise the transformer architecture [5, 26, 37, 38]. On the other hand, the authors of [43] recognise that irregularity is a crucial feature of event sequences and, as such, should be taken into account. In turn, our method goes one step further, integrating this irregularity into the architecture itself.

More advanced works leverage TPP theory in combination with NNs. The article [42] introduces an approach for modelling event sequences with random timestamps that are asynchronously generated, utilising two RNNs. The authors of the paper [48] decided to apply the transformer architecture with some TPP-inspired modifications. As a downside, both of these methods have a very limited class of processes they can represent. Another intriguing paper in this field proposes continuous convolutions for modelling irregular processes [47]. Despite being more versatile, it requires extensive kernel training and is less sensitive to interval sizes.

Discontinuous-trajectory Neural ODEs. In contrast to classic, NN-based methods, we take care of irregularity more naturally. Using ODE theory, our model doesn’t simply account for the differences between intervals, but directly evolves over time instead.

This idea is taken from the original paper [10], which proposed to apply the novel Neural ODE method for generating time series. Consequently, it is well-suited for handling irregular event sequences. Building on this thought, the authors of [31] proposed using the same approach to model the evolution of the RNN’s hidden state between events, naming their method RNN-ODE.

Another branch of prospective research, inspired by the original paper, incorporates a continuous TPP-based loss into the Neural

ODE method. The authors of [19] use Neural Jump Stochastic Differential Equations (NJSDE) to model the evolution of $\mathbf{h}(t)$, which resembles RNN-ODE in everything except for memory cost and efficiency. The work [34] takes another step by additionally decoupling the trajectories of different events. This results in a significant speed-up due to parallelisation, along with improvements in quality. Building on the variational autoencoder idea, a recent paper [41] also proposed to integrate the event trajectories separately.

Another intriguing approach in this field was presented by [12], which utilised Gaussian Processes to account for missing features optimally. Notably, they also introduced a rather restrictive, basic version of negative feedback, motivating it by a difference equation. We build on that in our work, proposing a gentler solution.

Both the RNN-ODE and NJSDE-based methods account for the input sequence by introducing jumps at times of events. Consequently, the resulting paths are inherently discontinuous. We aim to fill this gap. We argue that if the events do not cause shocks to the modelled system, as with transactions or medical observations, they should not be modelled by jumps. Instead, we propose carefully building up the trajectory in anticipation of an event and gradually winding it down once it has occurred.

Continuous-trajectory Neural ODEs. The motivation for a continuous trajectory is supported by [21]: the considered underlying processes develop in continuous time, and so should the model. The authors designed an architecture based on the controlled differential equations (CDEs) theory, which imposes certain restrictions. For one, they only considered raw time series, i.e. observations of a continuous process. Furthermore, the influence of the input data on the resulting hidden trajectory is purely linear. Also, the NN that processes the current hidden state must output a matrix, necessitating a cubic memory footprint of the respective weights, so all their experiments are conducted on datasets with no more than 20 features, with embedding sizes ranging from 16 to 256. Finally, due to the reparametrisation invariance property of CDEs, the input sequence’s irregularity may be ignored since it cancels out anyway; it’s not taken into account without feeding the time intervals to the model along with the data. The last two points were also noted by the authors in their discussion section.

Gaussian process regression errors. The main part of our theoretical analysis involves the estimation of the squared error of an integral over a linear function of a Gaussian process with multiple outputs. Knowing little about the smoothness of separate output dimensions, we work with a smoothness upper bound, aiming for minimax error estimation. This assumption leads us to the generalisation of the results presented in [15, 45]. The authors provided the error bounds for Gaussian process interpolation with a single output. While alternatives exist [35, 36], including the model misspecification case [39, 46], they are not suitable for the generalisation under the minimax setting described above with an additional ODE layer on top.

Conclusion. We aim to fill the aforementioned gaps and introduce a novel continuous-trajectory model for processing event sequences. Unlike conventional approaches, our method is based on the Neural ODE framework to better model data irregularity. Compared to the previous results, the proposed solution does not impose any

restrictions on the utilised architectures. Additionally, it maintains reasonable memory requirements and exhibits faster calculations due to the absence of discontinuities in the integrated path. Finally, we also provide a theory-informed negative feedback modification, improving the model’s stability in theory and practice.

3 METHODS

In this section, we lay out the methods we propose in our work, as well as the theoretic background behind them.

3.1 COTODE pipeline

Our goal is to provide a representation $\mathbf{h}(t)$ in response to an input event sequence $\{c_k, t_k\}_{k=1}^n$, suitable for solving downstream problems. By $\{t_k\}_{k=1}^n \subset [0; T]$ we denote the timestamps of the input events, while $\{c_k\}_{k=1}^n$ denotes the types of these events.

To achieve this goal, we use a three-part pipeline, traditional for event sequences [3, 5]. The first layer is the Embedder, responsible for converting categorical features $\{c_k\}_k$ into vectors $\{\mathbf{x}_k\}_k$ using a learnable dictionary. Next, the Backbone runs on these vectors, returning a single embedding per sequence $\mathbf{h}(T)$. Finally, a linear head on top of the final hidden state $\mathbf{h}(T)$ transforms it into the prediction \hat{y} . The pseudocode for this approach is provided in Algorithm 1, complemented with an illustration in Figure 3.

Our backbone of choice is a Neural ODE-based architecture. It requires a function $\mathbf{x}(t) : [0; T] \rightarrow \mathbb{R}^d$, instead of a sequence $\{\mathbf{x}_k\}_k$. Here d is the dimensionality of the input embedding. The main contribution of this paper is an approach based on *Gaussian processes interpolation* that provides this continuous trajectory $\hat{\mathbf{x}}(t)$, for any given $t \in [0, T]$. It exhibits superior quality, as confirmed by both experimental and theoretical studies.

Then, the Neural ODE layer uses the Gated Recurrent Unit (GRU) [11] function as its dynamics. Given \mathbf{x}_t , it produces the trajectory $\mathbf{h}(t)$ that concludes with $\mathbf{h}(T)$. Negating \mathbf{h} here leads to greater numerical stability of the proposed approach, being a crucial part of our methodology.

Algorithm 1: The forward pass of the COTODE method. The backward pass is made by the Adjoint method from [10], combined with automatic differentiation from [2].

Input : $\{c_k, t_k\}_k$ — event data;
 $\mathbf{h}_0, \varepsilon$ — hyperparameters;
 Embedder(\cdot), Interpolate(\cdot) — predefined functions for data processing;
 Solver(\cdot) — ODE solver.

Output: $\mathbf{h}(T)$ — hidden state at final timestamp T .
 // ε — to take the last event into account.
 $T \leftarrow \max(\{t_k\}_k) + \varepsilon$;
 $\{\mathbf{x}_k\}_k \leftarrow \text{Embedder}(\{c_k\}_k)$;
 $\hat{\mathbf{x}}(\cdot) \leftarrow \text{Interpolate}(\{\mathbf{x}_k, t_k\}_k)$;
function Dynamics($\hat{\mathbf{x}}(\cdot), \mathbf{h}, t$):
 | // The sign $-$ is for negative feedback.
 | **return** GRU($\hat{\mathbf{x}}(t), -\mathbf{h}$);
end Dynamics
 $\mathbf{h}(T) \leftarrow \text{Solver}(\mathbf{h}_0, 0, T, \text{Dynamics}(\hat{\mathbf{x}}(\cdot), \cdot))$;
return $\mathbf{h}(T)$;

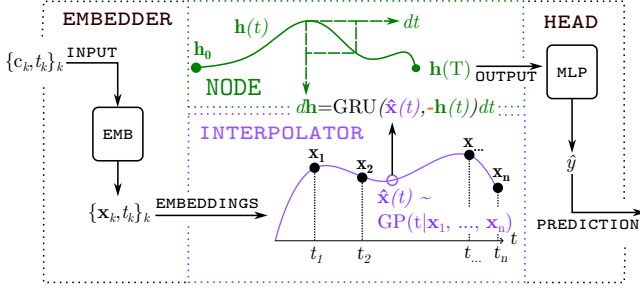


Figure 3: Scheme of the proposed COTODE method. The embedded input sequence $\{x_k, t_k\}_k$ is passed into the backbone, where it is interpolated via Gaussian Process Regression, and the result is then used to guide the Neural ODE trajectory. The minus sign $-$ denotes the introduced negative feedback. The final state of this trajectory is fed to a linear classifier, which is responsible for transforming it into predictions.

3.2 Neural ODE overview

The Neural ODE layer was first proposed by [10]. It propagates the hidden state by solving a Cauchy problem from a fixed starting point. The learnable parameters adjust the dynamics function’s behaviour within this problem. At first, the input data was used purely to alter the starting point.

Subsequent works, such as Neural CDEs [21], proposed to add a dependency on the input data interpolation function $\hat{x}(t)$ into the dynamics. We also follow this approach. Our method can formally be written as a Cauchy problem $\text{Ca}(\mathbf{h}_0, \mathbf{f}_\theta, \hat{x}(t))$:

$$\begin{aligned} \text{Dynamics: } & \begin{cases} \mathbf{h}(0) = \mathbf{h}_0; \\ \frac{d\mathbf{h}(t)}{dt} = \mathbf{f}_\theta(\mathbf{h}(t), \hat{x}(t), t). \end{cases} \\ \text{Solution: } & \mathbf{h}(t) : [0, T] \rightarrow \mathbb{R}^d. \end{aligned} \quad (1)$$

Here, \mathbf{h}_0 is a predefined starting point, \mathbf{f}_θ is a neural network, which defines the dynamics for $t \in [0, T]$. As mentioned above, since we are working with time series, the input is fed to the dynamics as an interpolation function of the input data $\hat{x}(t)$, instead of being encoded into \mathbf{h}_0 as is the case for Neural ODE methods on tabular data. As a result of integrating these dynamics, we obtain our target $\mathbf{h}(T)$ — the hidden state at the final timestamp T .

3.3 Interpolation of the hidden trajectory

We note that to continuously model the hidden trajectory, it is necessary to define the influence that events have on it in the gaps between them. The Neural CDE method [21] processes the input data as-is. Since direct usage of categorical features as inputs makes no sense, we first embed all such features into learnable vectors and then apply the proposed interpolation approach.

Below, we provide a Gaussian Process-based model for the data interpolation function $\hat{x}(t)$. Taking advantage of the theory behind this method, we can devise error bounds for the final hidden state.

3.3.1 Practical aspects of Gaussian Processes. Here, we will discuss the basic theory behind this approach, which we will use in practice.

Let $\mathbf{x}(t)$ be a stationary zero-mean d -dimensional Gaussian process (GP) with the covariance function $\mathbf{K}(\cdot, \cdot) = \{K_i(\cdot, \cdot)\}$ and independent components:

$$\mathbb{E}\mathbf{x}(t) \equiv \mathbf{0}; \quad \mathbb{E}[\mathbf{x}(t_1) \odot \mathbf{x}(t_2)] = \mathbf{K}(t_1, t_2) \equiv \mathbf{K}(t_2 - t_1), \quad (2)$$

where the symbol \odot is used to denote component-wise multiplication.

Suppose we also know the values of said process at timestamps $\{t_1, \dots, t_n\} \subset [0, T]$, and we wish to build a linear prediction $\hat{x}(t)$:

$$\mathbf{x}(t_i) = \mathbf{x}_i, \quad i = 1, \dots, n \implies \hat{\mathbf{x}}(t) = \sum_{i=1}^n a_i \mathbf{x}_i. \quad (3)$$

The choice of the coefficients $\mathbf{a} = \{a_i\}_{i=1}^n$ is guided by the minimization of the mean squared error σ^2 :

$$\sigma^2(t) \triangleq \mathbb{E}\|\hat{\mathbf{x}}(t) - \mathbf{x}(t)\|^2. \quad (4)$$

In our experiments, when calculating $\hat{x}(t)$, we use a well-known result [7], which corresponds to the maximum a posteriori estimation:

$$\mathbf{a} = K^{-1}\mathbf{k}, \quad (5)$$

where K is the covariance matrix, \mathbf{k} is the covariance vector, and $\mathbf{K}(t)$ is a standard squared exponential covariance function, identical over all dimensions (α is a hyperparameter, we refer to as *scale*):

$$\mathbf{K}(t) = (e^{-\alpha t^2}, \dots, e^{-\alpha t^2}). \quad (6)$$

We set $\alpha = 1$ in most cases; further details on tuning it may be found in Appendix C.

3.3.2 Gaussian Process error estimation.

Plan. We do not observe the client in-between events, which means that \hat{x} is only our most probable estimate. GP interpolation is a well-studied, theory-backed method, which allows us to quantify the uncertainty of estimating \hat{x} . This uncertainty is then accumulated in the hidden state due to integration, and our aim in this section is to assess the impact this has on $\mathbf{h}(T)$. Our main result may be informally written as follows:

THEOREM. (informal) *The estimation error of the final hidden state $\mathbf{h}(T)$ follows the asymptotic:*

$$\begin{aligned} (n-1)\delta_{\min}^2 & \lesssim \int_0^T \mathbb{E} \left\| \frac{\mathbf{h}(t)}{dt} - \frac{\mathbf{h}^*(t)}{dt} \right\|^2 dt \lesssim (n-1)\delta_{\max}^2, \\ \|\mathbf{h}(T) - \mathbf{h}^*(T)\|^2 & \lesssim (n-1)\delta_{\max}^2, \end{aligned}$$

where $\delta_{\min}, \delta_{\max}$ are the length of the minimum and maximum intervals between events, and $n-1$ is the total number of these intervals, $\mathbf{h}^*(t)$ is the trajectory that corresponds to the true \mathbf{x} .

This would imply that without additional regularization, the error grows approximately linearly with time as we observe more events. Below, we provide the formal statements with their proofs.

Error definition. First, let us define the *total integral error*:

$$\sigma_{\text{ALL}}^2 = \int_0^T \mathbb{E}\|\hat{\mathbf{x}}(t) - \mathbf{x}(t)\|^2 dt. \quad (7)$$

Uniform theoretic bounds. The form of the estimator given by (5) is useless when it comes to establishing the bounds for (7): it is tough to deal with the inverse form of K . This forces us to approach the problem from a different angle, following existing results on estimating the GP regression error [45]. To use these prior results, we have to consider a more convenient intermediate form of the error, integrated between two events:

$$\sigma_{\text{INT}}^2(k) = \int_{t_k}^{t_{k+1}} \mathbb{E} \|\hat{\mathbf{x}}(t) - \mathbf{x}(t)\|^2 dt. \quad (8)$$

Assumption and their effect on the error. We first devise error bounds for a uniform sequence and generalize them later to our irregular case. Formally, we make two common assumptions, which, as will be explained below, do not reduce the applicability of the devised results:

ASSUMPTION 1. *The data lies on a regular grid with a step size $\delta > 0$:*

$$t_k = t_0 + k\delta, k = 1, \dots, n.$$

ASSUMPTION 2. *The input sequence is infinite:*

$$k = -\infty, \dots, -2, -1, 0, 1, 2, \dots, +\infty.$$

Assumption 1 can be made without loss of generality. The error for a uniform grid can be extended to the case of irregular event sequences using the following lemma.

LEMMA 3.1. *Let $S = \{(\mathbf{x}_k, t_k)\}_{k=1}^n$ be a given irregular event sequence. We construct an alternative event sequence $\tilde{S} = \{(\mathbf{x}_k, \tilde{t}_k)\}_{k=1}^n$, with the interval $[m; m+1]$ changed by r , for some fixed $1 \leq m < k$ and $r \in \mathbb{R}$:*

$$\begin{cases} \tilde{t}_k = t_k, k \leq m; \\ \tilde{t}_k = t_k + r, k > m; \\ \tilde{t} = t + \mathbb{I}[t > t_{m+1}]r. \end{cases}$$

Here \mathbb{I} denotes the indicator function. Then, the errors (8) for the original S and modified \tilde{S} sequences (σ^2 and $\tilde{\sigma}^2$ respectively) relate as follows:

$$\begin{aligned} \sigma^2(t) &\leq \tilde{\sigma}^2(\tilde{t}) \text{ for } r > 0, \\ \sigma^2(t) &\geq \tilde{\sigma}^2(\tilde{t}) \text{ for } r < 0. \end{aligned}$$

This lemma allows us to extend our results to irregular sequences without loss of generality. It is evident if one considers the problem from the perspective of probability theory. The respective covariance determines the amount of information each observation provides about the unknown value. If all covariances decrease, the variance of $\hat{\mathbf{x}}$ will clearly increase and vice versa. As a corollary, the transition to a uniform sequence with the largest time interval as the step δ_{max} may only increase the error, and with the smallest δ_{min} – decrease, so any upper or lower bounds we prove in the regular case will still be valid (for extreme step sizes).

As for Assumption 2, the authors of [45] demonstrated that these results empirically hold for finite sequences. Indeed, since a typical kernel decays with an exponential speed, distant observations have a negligible impact on the resulting error.

Together, these assumptions may be formally written as follows:

$$t_k = k\delta; \forall k \in \mathbb{Z}. \quad (9)$$

Error bound for the optimal estimator. The optimal estimator for a uniform infinite grid is well-known [22], and is much simpler than (5):

$$\hat{\mathbf{x}}(t) = \delta \sum_{k=-\infty}^{\infty} \mathbf{K}(t - k\delta) \mathbf{x}(k\delta). \quad (10)$$

This form allows us to deduce analytical error bounds. For this purpose, we generalize the results from [45] to multiple dimensions. This is given by the following Lemma.

LEMMA 3.2. (proof in Appendix A) *Let $F(\omega)$ denote the spectral density of Gaussian process from (2):*

$$F(\omega) = \int_{-\infty}^{\infty} \exp(2\pi i \omega t) \mathbf{K}(t) dt.$$

In this notation, under Assumptions 1,2 the following holds:

$$\mathbb{E} \|\hat{\mathbf{x}}(t) - \mathbf{x}(t)\|^2 = d \int_{-\infty}^{\infty} F(\omega) \left| 1 - \sum_{k \neq 0} e^{2i\pi\omega(t-t_k)} K(t-t_k) \right|^2 d\omega.$$

With Lemma 3.2, all other results can be taken directly from [45], taking into account that $\mathbf{x}(t)$ is d -dimensional. We recount select findings from this paper: the general error form, an analytic error expression for a specific kernel analogous to (6), and the minimax error bound.

THEOREM 3.3. *The error (8) may be written in the following form:*

$$\sigma_{\text{INT}}^2 = d\delta \int_{-\infty}^{\infty} F(\omega) \left((1 - \hat{K}(\omega))^2 + \sum_{k=-\infty}^{\infty} \hat{K}\left(\omega + \frac{k}{\delta}\right) \right) d\omega. \quad (11)$$

Note that the error (11) does not depend on the interval number. This is due to the inherent symmetry of an infinite uniform grid: all intervals are the same in terms of the covariance function.

ASSUMPTION 3. *The covariance function is the same over all dimensions and corresponds to the squared exponential function:*

$$K(t) = \sqrt{2\pi} e^{-2(\alpha\pi t)^2}.$$

COROLLARY 3.4. *Under the Assumptions 1–3, the error (11) can be bounded analytically:*

$$\begin{cases} \sigma_{\text{INT}}^2 \leq d \cdot 7\delta^2 \alpha \exp\left(-\frac{1}{8(\delta\alpha)^2}\right) \triangleq D_0^{\text{max}}(\delta), \\ \sigma_{\text{INT}}^2 \geq d \cdot \frac{4}{3}\delta^2 \alpha \exp\left(-\frac{1}{8(\delta\alpha)^2}\right) \triangleq D_0^{\text{min}}(\delta), \end{cases} \quad (\delta\alpha \rightarrow 0). \quad (12)$$

Error bound for the optimal estimator in the minimax case. On the other hand, we may also use a more general approach to determining the covariance function \mathbf{K} , independent of the specific kernel, since it may be unknown or may vary between dimensions. It leads us to the following Assumption:

ASSUMPTION 4. *All the spectral densities of \mathbf{K} belong to the following class of functions:*

$$\mathcal{F}(L) = \left\{ F : \mathbb{E} \left(\frac{\partial x_F(t)}{\partial t} \right)^2 \leq L \right\}. \quad (13)$$

Then, we can generalize results from [45] for the multivariate case.

THEOREM 3.5. *In the above notation, under the Assumptions 1,2,4, the minimax GP interpolation error may be calculated analytically:*

$$R^h(L) \triangleq \inf_{\hat{\mathbf{x}}} \sup_{F \in \mathcal{F}(L)} \sigma_{INT}^2 = \frac{L\delta^2 d}{2\pi^2} \triangleq D_1(\delta). \quad (14)$$

Finally, combining Lemma 3.1 with Corollary 3.4 or Theorem 3.5 (depending on assumptions about \mathbf{K}) and transitioning to the finite irregular case with $n - 1$ intervals (with δ_{\min} for $D_{0,1}^{\min}$ and δ_{\max} for $D_{0,1}^{\max}$), we achieve the following inequalities for the upper bound of the total error:

$$\begin{aligned} \sigma_{ALL}^2 &\in [(n-1)D_0^{\min}, (n-1)D_0^{\max}] \quad (\text{under Assumption 3}), \\ \sigma_{ALL}^2 &\in [(n-1)D_1^{\min}, (n-1)D_1^{\max}] \quad (\text{under Assumption 4}). \end{aligned} \quad (15)$$

Neural ODE Error. Now, we can apply the above findings to our task. Let us consider two variants of the Cauchy problem (1): one with a "true" signal $\mathbf{x}(t)$, and the other with a signal, reconstructed from observations via GP interpolation $\hat{\mathbf{x}}(t)$. We will denote their hidden trajectories as $\mathbf{h}^*(t), \mathbf{h}(t)$ respectively. Then, the difference between the resulting hidden states, accumulated during integration, is written as:

$$\begin{aligned} \sigma_{\mathbf{h}}^2 &\triangleq \int_0^T \mathbb{E} \left\| \frac{d\mathbf{h}^*}{dt} - \frac{d\mathbf{h}}{dt} \right\|^2 dt = \\ &= \int_0^T \mathbb{E} \left\| \mathbf{f}_{\theta}(\mathbf{x}, \mathbf{h}^*, t) - \mathbf{f}_{\theta}(\hat{\mathbf{x}}, \mathbf{h}, t) \right\|^2 dt. \end{aligned} \quad (16)$$

To bound this error, it is necessary to restrict the class of functions \mathbf{f}_{θ} .

ASSUMPTION 5. *Let the functions \mathbf{f}_{θ} be confined to linear bi-Lipshitz functions of \mathbf{x} with parameters being a matrix W_x :*

$$\mathbf{f}(\mathbf{x}) = W_x \mathbf{x}; \quad 0 < \lambda_{\min}(W_x) < \lambda_{\max}(W_x), \quad (17)$$

where $\lambda_{\min}, \lambda_{\max}$ are the minimal and the maximal eigenvalues of W_x .

Note that we also removed the dependence on t : this can be done without additional limitations by concatenating t to $\hat{\mathbf{x}}$. Altogether, this allows us to deduce the following:

THEOREM 3.6. *(proof in Appendix A) Consider the task (1) under Assumption 5. Then, the following holds:*

(1) *If the covariance function has the form from Assumption 3, the interpolation error from (16) adheres to the following bound:*

$$(n-1)\lambda_{\min}(W_x)D_0^{\min} \leq \sigma_{\mathbf{h}}^2 \leq (n-1)\lambda_{\max}(W_x)D_0^{\max}.$$

(2) *Otherwise, if the covariance function satisfies Assumption 4, the corresponding minimax interpolation error can be calculated directly:*

$$(n-1)\lambda_{\min}(W_x)D_1^{\min} \leq \sigma_{\mathbf{h}}^2 \leq (n-1)\lambda_{\max}(W_x)D_1^{\max}.$$

Besides, both of the above upper-bounds are also true for the difference between the final hidden states:

$$\|\mathbf{h}(T) - \mathbf{h}^*(T)\|^2 \leq \sigma_{\mathbf{h}}^2 \leq (n-1)\lambda_{\max}(W_x)\{D_0^{\max}, D_1\}$$

Using this approach, we are able to quantify the uncertainty from not knowing what happens in-between events, accumulated in the final hidden state.

3.4 GRU Negative feedback

The error bound from Theorem 3.6 leads to disappointing conclusions: the error grows linearly with sequence length. This corresponds to the exploding gradients problem, well-studied for discrete sequential models [17], and we propose solving it in the continuous case with a negative feedback procedure.

3.4.1 Theoretical consideration. First, we will discuss the theoretical benefits of this procedure. Consider the following scenario: two trajectories $\mathbf{h}(t), \mathbf{h}^*(t)$ have the same dynamics, but distinct starting states $\mathbf{h}_0 \neq \mathbf{h}_0^*$ at timestamp $t = 0$. This is meant to imitate the difference between the true and the estimated trajectory: the estimated trajectory accumulated errors during its evolution until $t = 0$ but adhered to the correct dynamics afterwards. Formally, this is described by a simple ODE on the interval $[0, T]$:

$$\frac{d\mathbf{h}}{dt} = W_h \mathbf{h}; \quad \frac{d\mathbf{h}^*}{dt} = W_h \mathbf{h}^*, \quad (18)$$

where W_h is the parameter matrix. If W_h is negative-definite, the difference between those states, according to the matrix ODE theory, will decrease exponentially.

LEMMA 3.7. *(proof in Appendix A) Let $\mathbf{h}_0 \neq \mathbf{h}_0^*$ be two non-equal starting points for two Cauchy problems $\text{Ca}(\mathbf{h}_0, W_h \mathbf{h})$ and $\text{Ca}(\mathbf{h}_0^*, W_h \mathbf{h}^*)$. For the negative-definite matrix $W_h < 0$ with eigenvalues $\lambda_i < 0$ for some constants C_i the following holds:*

$$\|\mathbf{h}(T) - \mathbf{h}^*(T)\| \leq \sum_i C_i e^{-|\lambda_i|T}. \quad (19)$$

3.4.2 Negative Feedback in practice. The aforementioned problem of the linearly growing error arises from the additive nature of differential equations. The empirical solvers we use share this nature, and as such, this issue also manifests itself in our study's experimental results.

As a consequence of the above theory, it is beneficial to enforce the weight matrix, which corresponds to \mathbf{h} , to be negative-definite. In practice, prior works have solved this by forcing the derivative to point toward decreasing the hidden state. For example, the authors of [12] simply subtract the hidden state from the derivative. Indeed, for a matrix of limited spectral norm (as is often the case due to L_2 regularization), this results in the following modification:

$$\tilde{W}_h = W_h - I \implies \lambda_{\max}(\tilde{W}_h) = \lambda_{\max}(W_h) - 1 \lesssim 0.$$

We developed a more holistic solution inspired by the GRU architecture [11]:

$$\mathbf{r} = \sigma(W_{ir}\mathbf{x} + \mathbf{b}_r + W_{hr}\mathbf{h} + \mathbf{b}_{hr}), \quad (20)$$

$$\mathbf{z} = \sigma(W_{iz}\mathbf{x} + \mathbf{b}_z + W_{hz}\mathbf{h} + \mathbf{b}_{hz}), \quad (21)$$

$$\mathbf{n} = \tanh(W_{in}\mathbf{x} + \mathbf{b}_{in} + \mathbf{r} \odot (W_{nh}\mathbf{h} + \mathbf{b}_{nh})), \quad (22)$$

$$\tilde{\mathbf{h}} = (1 - \mathbf{z}) \odot \mathbf{n} + \mathbf{z} \odot \mathbf{h}. \quad (23)$$

We noticed that by negating the second term in (23), since \mathbf{z} is positive, one can achieve, in essence, a learnable negative feedback effect.

Moreover, this can be done without modifying the GRU architecture by simply negating \mathbf{h} before passing it to this layer. This way, the terms that contain \mathbf{h} in (20), (21), (22) will simply need to learn a negative version of the weights, which makes this equivalent to the proposed architecture modifications. All in all, this allows us to

maintain the norm of the resulting embeddings within reasonable limits without putting severe constraints on the hidden trajectory.

4 EXPERIMENTS

In this section, we provide our empirical results, demonstrating the superiority of the proposed models in practice. To this end, we first outline the experiment settings (our datasets and the models we compare), followed by the results and the corresponding discussion.

4.1 Data

The datasets in question have one label per sequence, summarising it in one way or another. Four out of six of our datasets are transactional, mostly because they are abundant, similar in format and thus easy to work with. A transaction consists of a continuous amount feature, a categorical MCC-code feature (transaction type, e.g., ATM deposit/withdrawal, payment at retail clothing, etc.), and a timestamp. All transactions are grouped by bank clients. Consequently, these datasets differ only in their target labels.

- The *Age* dataset [32] has the client’s age as its label. It is grouped into four bins for convenience.
- The *Churn* dataset [30] poses the binary classification task, with the positive label indicating the client will leave the bank.
- The *HSBC* competition [28] poses the fraud identification task, with one label per transaction. For consistency with other tasks, we defined a clientwise label, indicating whether any of a client’s transactions were fraudulent.
- The *Gender* dataset [33] poses the task of binary classification, with the client’s gender as its label.

Besides, we also used two non-transactional datasets to demonstrate the wide applicability of our method. They required some specific data preprocessing, described in Appendix B.

- The *WISDM* Human Activity Classification dataset [40] contains records of various human activities. The features here are the coordinates and accelerations of two devices: a phone and a watch. The label corresponds to one of 18 possible activities.
- The *Retail* dataset [9] has records of online retail purchases from a UK-based and registered store.

In all the datasets except for Retail and Gender, we only considered sequences longer than 32 but shorter than 800. For the remaining two, we allowed sequences as short as 16 elements for the Retail dataset and as short as four elements for the Gender dataset.

As all our datasets have a multiclass classification target, we use class-weighted ROC AUC and micro-averaged accuracy as the quality metrics.

4.2 Models

In our empirical study, we compared the performance of six models. The considered models are all, in essence, some modification of the GRU architecture [11], including the raw GRU model itself. We have two reasons for focusing on recurrent architectures instead of transformers: there is a lack of research on their continuous implementations and they are shown to be inferior in empirical comparative studies [5, 47].

Below is a list of the considered models with brief descriptions, ordered in increasing complexity.

- RNN [11]: the vanilla GRU architecture;
- RNN Decay [23]: the architecture, which decays the hidden state exponentially in between events;
- RNN ODE [31]: the architecture that models inter-event dynamics via an ODE and induces jumps at times of events using an RNN.
- COTODE: the proposed GP-based method, along with two alternative ablation study approaches with differing interpolation regimes.
 - GP: the Gaussian Process-based regime, our method;
 - Last: interpolation using the last seen embedding, ablation study variation;
 - Decay: exponentially decaying sum of prior events, ablation study variation.

The categorical features are encoded into learnable embeddings for all considered models and then concatenated with numerical features. Notably, we also appended the time since the last transaction to this vector. This evens the playing field for the raw RNN model, allowing it to take irregularity into account.

All the code for our experiments is written in Python, using the PyTorch software package [2], in combination with the PyTorch Lightning framework [13]. Creating and solving neural differential equations was done via the TorchODE library [24]. For convenient experiment management, we employed the Hydra framework [44], combined with WandB for logging [6]. All our code and the used parameters can be accessed through GitHub¹.

4.3 Results

The results for the transactional datasets are presented in Table 1. Our method demonstrates exceptional performance, surpassing other models on three out of four datasets. On the Gender dataset, our models achieve a close second, only being outperformed by the RNN method. We hypothesise that this is because the sequences are too short for the ODE methods to accumulate meaningful information.

Besides transactional datasets, to illustrate the wide applicability of these methods, we also provide the results on two non-transactional datasets. These results are given by Table 2.

The Human Activity Classification task, despite not being a true event-sequence scenario, also prefers our proposed methods. The proposed approach outperforms the standard RNN method, even with regularly spaced observations. We hypothesise that this is due to a larger *virtual depth* of the Neural ODEs: they have greater control over the hidden trajectory and, as such, are able to model dynamics of higher complexity.

On the other hand, the Retail dataset favours the vanilla model. Again, as was the case with Gender, this is most likely due to the short length of the input sequences.

Besides the metrics, we also illustrated the resulting paths for our GP-based Neural ODE in figure 2. The hidden trajectory was sampled at 100 uniform points and cast to two dimensions using PCA. The generated curve has complex dynamics and does not

¹https://anonymous.4open.science/r/cotode_kdd2025-B284/

Table 1: Experimental results on transactional datasets. The results are averaged over three runs and are given in the format $mean \pm std$. Best values are highlighted with bold font, second best —underlined.

Dataset	Backbone	ROC AUC	Accuracy
Age	RNN	0.75 ± 0.01	0.47 ± 0.02
	RNN Decay	0.50 ± 0.00	0.00 ± 0.00
	RNN ODE	0.63 ± 0.01	0.43 ± 0.03
	COTODE Last	0.75 ± 0.01	0.52 ± 0.03
	COTODE Decay	0.68 ± 0.03	0.41 ± 0.01
	COTODE GP	0.75 ± 0.02	<u>0.48 ± 0.02</u>
Churn	RNN	0.65 ± 0.01	0.65 ± 0.02
	RNN Decay	0.68 ± 0.01	0.66 ± 0.00
	RNN ODE	0.53 ± 0.03	0.62 ± 0.00
	COTODE Last	<u>0.78 ± 0.01</u>	0.73 ± 0.00
	COTODE Decay	<u>0.76 ± 0.02</u>	<u>0.70 ± 0.01</u>
	COTODE GP	0.79 ± 0.00	0.73 ± 0.00
HSBC	RNN	0.53 ± 0.03	0.95 ± 0.00
	RNN Decay	0.55 ± 0.01	0.95 ± 0.00
	RNN ODE	0.49 ± 0.03	0.95 ± 0.00
	COTODE Last	0.54 ± 0.11	0.95 ± 0.00
	COTODE Decay	0.64 ± 0.01	0.94 ± 0.00
	COTODE GP	0.58 ± 0.08	0.95 ± 0.00
Gender	RNN	0.71 ± 0.01	0.67 ± 0.00
	RNN Decay	0.57 ± 0.00	0.60 ± 0.01
	RNN ODE	0.51 ± 0.02	0.55 ± 0.00
	COTODE Last	0.65 ± 0.01	0.63 ± 0.01
	COTODE Decay	0.60 ± 0.03	0.59 ± 0.01
	COTODE GP	<u>0.67 ± 0.00</u>	<u>0.64 ± 0.01</u>

Table 2: Experimental results on non-transactional datasets. The results are averaged over three runs and are given in the format $mean \pm std$. Best values are highlighted with bold font, second best —underlined.

Dataset	Backbone	ROC AUC	Accuracy
WISDM	RNN	0.81 ± 0.01	0.28 ± 0.01
	RNN Decay	0.79 ± 0.01	0.23 ± 0.01
	RNN ODE	0.76 ± 0.01	0.15 ± 0.01
	COTODE last	<u>0.88 ± 0.01</u>	0.40 ± 0.02
	COTODE Decay	0.82 ± 0.02	0.26 ± 0.03
	COTODE GP	0.89 ± 0.00	<u>0.36 ± 0.02</u>
Retail	RNN	0.91 ± 0.00	0.95 ± 0.01
	RNN Decay	<u>0.86 ± 0.01</u>	0.91 ± 0.01
	RNN ODE	0.48 ± 0.07	0.91 ± 0.00
	COTODE last	0.70 ± 0.03	0.91 ± 0.00
	COTODE Decay	0.64 ± 0.05	0.91 ± 0.00
	COTODE GP	0.82 ± 0.04	0.91 ± 0.00

collapse into trivial cases. This indicates that the resulting path is truly informative of the actor’s state.

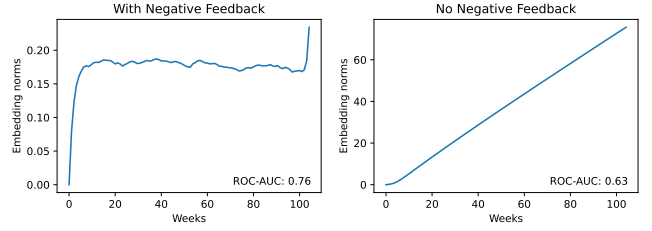


Figure 4: Dynamics of the hidden trajectory’s norm: with negative feedback (left), and without (right).

4.4 Ablation Study

4.4.1 Negative Feedback. To study the effect of the GRU-based negative feedback, we evaluated the embeddings’ norms across the whole trajectory, with and without the proposed modification (negation of h). These experiments were done on the Age dataset. The results are presented in Figure 4. Without any intervention, the trajectory’s norm grows linearly with time, which is definitely not the desired behaviour. The proposed modification clearly solves this issue, with the norm quickly reaching a certain balance instead of increasing uncontrollably along the entire trajectory.

Besides, we also provide the readers with the resulting ROC-AUC metrics for these model variants in the lower right corner of the graphs in Figure 4. The metrics clearly favour the version which uses the proposed negative feedback modifications, with a significant 20% gap (0.76 vs 0.63).

4.4.2 Other interpolation regimes. As mentioned above, we also considered two other interpolation regimes, specifically interpolation by the last event (COTODE last) and interpolation by exponential decay of prior events (COTODE Decay). The results for these models are given alongside our main experimental study in Tables 1,2. These models often performed on-par with the Gaussian Process-based approach. However, they show significant drops in quality on some datasets, while outperforming GP on others.

5 CONCLUSIONS

In this article, we present a fresh perspective on the task of analysing event sequences. By considering the influence of events in the intervals between them, we gain the ability to work with these sequences in a manner akin to continuous time series. Inspired by this insight, we propose a corresponding modification to the Neural ODE model: we interpolate the input data sequence via Gaussian Processes, achieving an uninterrupted influence on the dynamics. This method outperforms all previously considered methods on sufficiently long sequences by up to 20% ROC-AUC.

Moreover, our primary theoretical contribution lies in defining error bounds for the proposed modification, establishing the uncertainty arising from clients’ unknown actions between events. These obtained estimates allow us to reveal a fundamental flaw within these methods: the error increases linearly over time. We demonstrate that this issue can be theoretically addressed using negative feedback. To this end, we also develop an elegant zero-cost solution, which represents a sufficiently novel and modern challenge in this field and limits the growth of error in practice.

REFERENCES

- [1] Maher Ala'raj, Maysam F Abbod, Munir Majdalawieh, and Luay Jum'a. 2022. A deep learning model for behavioural credit scoring in banks. *Neural Computing and Applications* 34, 8 (April 2022), 5839–5866. <https://doi.org/10.1007/s00521-021-06695-z>
- [2] Jason Ansel and Pytorch 2 team. 2024. PyTorch 2: Faster Machine Learning Through Dynamic Python Bytecode Transformation and Graph Compilation. In *29th ACM International Conference on Architectural Support for Programming Languages and Operating Systems, Volume 2 (ASPLOS '24)*. ACM. <https://doi.org/10.1145/3620665.3640366>
- [3] Dmitrii Babaev, Nikita Ovsov, Ivan Kireev, Maria Ivanova, Gleb Gusev, Ivan Nazarov, and Alexander Tuzhilin. 2022. CoLES: Contrastive Learning for Event Sequences with Self-Supervision. In *Proceedings of the 2022 International Conference on Management of Data (Philadelphia PA USA)*. ACM, New York, NY, USA. <https://doi.org/10.1145/3514221.3526129>
- [4] Dmitrii Babaev, Maxim Savchenko, Alexander Tuzhilin, and Dmitrii Umerenkov. 2019. ET-RNN: Applying deep learning to credit loan applications. In *Proceedings of the 25th ACM SIGKDD international conference on knowledge discovery & data mining (Anchorage AK USA)*. ACM, New York, NY, USA, 2183–2190. <https://doi.org/10.1145/3292500.3330693>
- [5] Alexandra Bazarova, Maria Kovaleva, Ilya Kuleshov, Evgenia Romanenkova, Alexander Stepikin, Alexandr Yugay, Dzhambulat Mollaev, Ivan Kireev, Andrey Savchenko, and Alexey Zaytsev. 2024. Universal representations for financial transactional data: embracing local, global, and external contexts. *arXiv preprint arXiv:2404.02047* (2024). <https://doi.org/10.48550/arXiv.2404.02047>
- [6] Lukas Biewald. 2020. Experiment Tracking with Weights and Biases. <https://www.wandb.com/>
- [7] Christopher M Bishop and Nasser M Nasrabadi. 2006. *Pattern recognition and machine learning*. Vol. 4. Springer.
- [8] Evgeniy Burnaev, Maxim Panov, and Alexey Zaytsev. 2016. Regression on the basis of nonstationary Gaussian processes with Bayesian regularization. *Journal of Communications Technology and Electronics* 61 (2016), 661–671. <https://doi.org/10.1134/S1064226916060061>
- [9] Daqing Chen. 2019. Online Retail II. UCI Machine Learning Repository. <https://doi.org/10.24432/C5CG6D>
- [10] Ricky TQ Chen, Yulia Rubanova, Jesse Bettencourt, and David K Duvenaud. 2018. Neural ordinary differential equations. *Advances in NeurIPS* 31 (2018).
- [11] Junyoung Chung, Caglar Gulcehre, Kyunghyun Cho, and Yoshua Bengio. 2014. Empirical evaluation of gated recurrent neural networks on sequence modeling. In *NIPS 2014 Workshop on Deep Learning, December 2014*.
- [12] Edward De Brouwer, Jaak Simm, Adam Arany, and Yves Moreau. 2019. GRU-ODE-Bayes: Continuous modeling of sporadically-observed time series. *Advances in NeurIPS* 32 (2019).
- [13] William Falcon and The PyTorch Lightning team. 2019. *PyTorch Lightning*. <https://doi.org/10.5281/zenodo.3828935>
- [14] Joseph Futoma, Sanjay Hariharan, and Katherine Heller. 2017. Learning to detect sepsis with a multitask Gaussian process RNN classifier. In *Proceedings of the 34th International Conference on Machine Learning*. PMLR, 1174–1182. <https://proceedings.mlr.press/v70/futoma17a>
- [15] Georgii Golubev and Ekaterina Krymova. 2013. On interpolation of smooth processes and functions. *Problems of Information Transmission* 49, 2 (2013), 127–148. <https://doi.org/10.1134/S0032946013020038>
- [16] Alan G Hawkes. 1971. Spectra of some self-exciting and mutually exciting point processes. *Biometrika* 58, 1 (1971), 83–90. <https://doi.org/10.1093/biomet/58.1.83>
- [17] Sepp Hochreiter and Jürgen Schmidhuber. 1997. Long short-term memory. *Neural computation* 9, 8 (1997), 1735–1780. <https://doi.org/10.1162/neco.1997.9.8.1735>
- [18] Alexander Ihler, Jon Hutchins, and Padhraic Smyth. 2006. Adaptive event detection with time-varying poisson processes. In *Proceedings of the 12th ACM SIGKDD International Conference on Knowledge Discovery and Data Mining*. 207–216. <https://doi.org/10.1145/1150402.115042>
- [19] Junteng Jia and Austin R Benson. 2019. Neural jump stochastic differential equations. *Advances in NeurIPS* 32 (2019).
- [20] Alistair EW Johnson, Tom J Pollard, Lu Shen, Li-wei H Lehman, Mengling Feng, Mohammad Ghassemi, Benjamin Moody, Peter Szolovits, Leo Anthony Celi, and Roger G Mark. 2016. MIMIC-III, a freely accessible critical care database. *Scientific data* 3, 1 (2016), 1–9. <https://doi.org/10.1038/sdata.2016.35>
- [21] Patrick Kidger, James Morrill, James Foster, and Terry Lyons. 2020. Neural controlled differential equations for irregular time series. *Advances in NeurIPS* 33 (2020), 6696–6707.
- [22] Andrey Kolmogorov. 1941. Interpolation and extrapolation of stationary random sequences. *Izvestiya Rossiiskoi Akademii Nauk. Seriya Matematicheskaya* 5 (1941), 3. https://doi.org/10.1007/978-94-011-2260-3_28
- [23] Patrick J Laub, Thomas Taimre, and Philip K Pollett. 2015. Hawkes processes. *arXiv preprint arXiv:1507.02822* (2015). <https://doi.org/10.48550/arXiv.1507.02822>
- [24] Marten Lienen and Stephan Günnemann. 2022. torchode: A Parallel ODE Solver for PyTorch. In *The Symbiosis of Deep Learning and Differential Equations II, NeurIPS*. <https://openreview.net/forum?id=uiKVKTiUYB0>
- [25] Hongyuan Mei and Jason M Eisner. 2017. The neural Hawkes process: A neurally self-modulating multivariate point process. *Advances in NeurIPS* 30 (2017).
- [26] Viktor Moskvoretiskii, Dmitry Osin, Egor Shvetsov, Igor Udovichenko, Maxim Zhelmin, Andrey Dukhovny, Anna Zhimerikina, Albert Efimov, and Evgeny Burnaev. 2024. Self-Supervised Learning in Event Sequences: A Comparative Study and Hybrid Approach of Generative Modeling and Contrastive Learning. *arXiv preprint arXiv:2401.15935* (2024). <https://doi.org/10.48550/arXiv.2401.15935>
- [27] C Palm. 1943. Intensitätsschwankungen im Fernsprechverkehr, vol. 44 of Ericsson Technics. *Stockholm aktiebolaget LM Ericsson* (1943).
- [28] Ashis Parida and Samal Alyal. 2023. *HSBC ML Hackathon 2023*. Retrieved July 29, 2024 from <https://www.kaggle.com/datasets/ashisparida/hsbc-ml-hackathon-2023/data>
- [29] Daniel Perico. 2019. *Earthquakes*. Retrieved 2024-08-05 from <https://www.kaggle.com/datasets/danielpe/earthquakes>
- [30] Rosbank. 2018. *Rosbank Churn Competition. Boosters*. Retrieved July 29, 2024 from <https://boosters.pro/championship/rosbank1/overview>
- [31] Yulia Rubanova, Ricky TQ Chen, and David K Duvenaud. 2019. Latent ordinary differential equations for irregularly-sampled time series. *Advances in NeurIPS* 32 (2019).
- [32] Sberbank. 2020. *Sberbank Lessons from the Present. Open Data Science*. Retrieved July 29, 2024 from <https://ods.ai/competitions/sberbank-sirius-lesson/data>
- [33] Sberbank. 2022. *Sberbank Gender Competition. Kaggle*. Retrieved July 29, 2024 from <https://www.kaggle.com/datasets/nenriki/sberbank-gender-prediction>
- [34] Yujee Song, LEE Donghyun, Rui Meng, and Won Hwa Kim. 2023. Decoupled Marked Temporal Point Process using Neural Ordinary Differential Equations. In *The Twelfth International Conference on Learning Representations*.
- [35] Michael L Stein. 2012. *Interpolation of spatial data: some theory for kriging*. Springer Science & Business Media.
- [36] AW van der Vaart and JH van Zanten. 2008. Rates of contraction of posterior distributions based on Gaussian process priors. *Annals of Statistics* 36, 3 (2008), 1435–1463. <https://doi.org/10.1214/009053607000000613>
- [37] Chongren Wang, Dongmei Han, Qigang Liu, and Suyuan Luo. 2018. A deep learning approach for credit scoring of peer-to-peer lending using attention mechanism LSTM. *IEEE Access* 7 (2018), 2161–2168. <https://doi.org/10.1109/ACCESS.2018.2887138>
- [38] Chongren Wang and Zhuoyi Xiao. 2022. A Deep Learning Approach for Credit Scoring Using Feature Embedded Transformer. *Applied Sciences (Basel)* 12, 21 (Oct. 2022), 10995. <https://doi.org/10.3390/app122110995>
- [39] Wenjia Wang and Bing-Yi Jing. 2022. Gaussian process regression: Optimality, robustness, and relationship with kernel ridge regression. *Journal of Machine Learning Research* 23, 193 (2022), 1–67. <http://jmlr.org/papers/v23/21-0570.html>
- [40] Gary Weiss. 2019. WISDM Smartphone and Smartwatch Activity and Biometrics Dataset. UCI Machine Learning Repository. DOI: <https://doi.org/10.24432/C5HK59>
- [41] Jingge Xiao, Leonie Basso, Wolfgang Nejdl, Niloy Ganguly, and Sandipan Sikdar. 2024. IVP-VAE: Modeling EHR Time Series with Initial Value Problem Solvers. In *Proceedings of the AAAI Conference on Artificial Intelligence*, Vol. 38. 16023–16031.
- [42] Shuai Xiao, Junchi Yan, Xiaokang Yang, Hongyuan Zha, and Stephen Chu. 2017. Modeling the intensity function of point process via recurrent neural networks. In *Proceedings of the AAAI conference on artificial intelligence*, Vol. 31. <https://doi.org/10.1609/aaai.v31i1.10724>
- [43] Yu Xie, Guanjuan Liu, Chungang Yan, Changjun Jiang, MengChu Zhou, and Maozhen Li. 2022. Learning Transactional Behavioral Representations for Credit Card Fraud Detection. *IEEE Transactions on Neural Networks and Learning Systems* PP (Oct. 2022), 1–14. <https://doi.org/10.1109/TNNLS.2022.3208967>
- [44] Omry Yadan. 2019. Hydra - A framework for elegantly configuring complex applications. Github. <https://github.com/facebookresearch/hydra>
- [45] Alexey Zaytsev and Evgeny Burnaev. 2017. Minimax approach to variable fidelity data interpolation. In *Artificial Intelligence and Statistics*. PMLR, 652–661. <https://proceedings.mlr.press/v54/zaytsev17a.html>
- [46] Alexey Zaytsev, Evgenya Romanenkova, and Dmitry Ermilov. 2018. Interpolation error of Gaussian process regression for misspecified case. In *Conformal and Probabilistic Prediction and Applications*. PMLR, 83–95. <https://proceedings.mlr.press/v91/zaytsev18a.html>
- [47] Vladislav Zhuzhel, Vsevolod Grabar, Galina Boeva, Artem Zabolotnyi, Alexander Stepikin, Vladimir Zholobov, Maria Ivanova, Mikhail Orlov, Ivan Kireev, Evgeny Burnaev, et al. 2023. Continuous-time convolutions model of event sequences. *arXiv preprint arXiv:2302.06247* (2023). <https://doi.org/10.48550/arXiv.2302.06247>
- [48] Simiao Zuo, Haoming Jiang, Zichong Li, Tuo Zhao, and Hongyuan Zha. 2020. Transformer Hawkes process. In *International conference on machine learning*. PMLR, 11692–11702. <https://proceedings.mlr.press/v119/zuo20a>

A PROOFS

PROOF. Proof of Lemma 3.2

Let us start with expanding the square:

$$\mathbb{E}\|\hat{\mathbf{x}}(t) - \mathbf{x}(t)\|^2 = \mathbb{E}[\hat{\mathbf{x}}^T(t)\hat{\mathbf{x}}(t)] - 2\mathbb{E}[\hat{\mathbf{x}}^T(t)\mathbf{x}(t)] + \mathbb{E}[\mathbf{x}^T(t)\mathbf{x}(t)].$$

Now, we consider the terms one by one, substituting (10) and rewriting in terms of spectral density. The first term gives:

$$\begin{aligned} \mathbb{E}[\hat{\mathbf{x}}^T(t)\hat{\mathbf{x}}(t)] &= h^2 d \sum_{k,l=-\infty}^{\infty} K(t-t_k)K(t-t_l)K(t_k-t_l) = \\ &= \int_{-\infty}^{\infty} F(\omega) \left(h^2 d \sum_{k=-\infty}^{\infty} K(t-t_k)K(t-t_l)e^{2\pi i\omega(t_l-t_k)} \right) d\omega. \end{aligned}$$

The second one:

$$\begin{aligned} 2\mathbb{E}[\hat{\mathbf{x}}^T(t)\mathbf{x}(t)] &= 2hd \sum_{k=-\infty}^{\infty} K^2(t-t_k) = \\ &= \int_{-\infty}^{\infty} F(\omega) \left(2hd \sum_{k=-\infty}^{\infty} K(t-t_k)e^{2\pi i\omega(t-t_k)} \right) d\omega. \end{aligned}$$

And, finally, the third one:

$$\mathbb{E}[\mathbf{x}^T(t)\mathbf{x}(t)] = K(0)d = d \int_{-\infty}^{\infty} F(\omega) d\omega.$$

Factoring out the spectral density integral, the remaining three terms are the expansion of the following modulus:

$$d \left| 1 + h \sum_{k=-\infty}^{\infty} K(t-t_k)e^{2\pi i\omega(t-t_k)} \right|^2.$$

□

PROOF. **Proof of Theorem 3.6** Consider the error (16):

$$\sigma_h^2 = \int_0^T \mathbb{E} \|W_x \mathbf{x}(t) - W_x \hat{\mathbf{x}}(t)\|^2 dt.$$

Applying prior results, we achieve:

$$\begin{aligned} \sigma_h^2 &\leq \int_0^T \|W_x(\hat{\mathbf{x}}(t) - \mathbf{x}(t))\|^2 dt \\ &\stackrel{(17)}{\leq} \int_0^T w \|(\hat{\mathbf{x}}(t) - \mathbf{x}(t))\|^2 dt \\ &\stackrel{(15)}{\leq} w(n-1)D_0^{\max} \end{aligned}$$

The last two inequalities are obtained using the \mathbf{f} function restrictions (17) and the bound on the total $\hat{\mathbf{x}}$ error (15). The remaining bounds can be devised similarly.

Finally, the upper bound on the difference between the final hidden states follows from bounding the integral norm by the integral of the norm:

$$\|\mathbf{h}^*(T) - \mathbf{h}(T)\|^2 = \left\| \int_0^T \left(\frac{d\mathbf{h}^*}{dt} - \frac{d\mathbf{h}(T)}{dt} \right) dt \right\|^2$$

$$\leq \int_0^T \left\| \frac{d\mathbf{h}^*}{dt} - \frac{d\mathbf{h}(T)}{dt} \right\|^2 dt$$

□

PROOF. Proof of Lemma 3.7

Consider the following Cauchy problem, which describes the difference $\Delta = \mathbf{h}(t) - \mathbf{h}^*(t)$ between the given Cauchy problems:

$$\begin{cases} \Delta(0) = \Delta_0 = \mathbf{h}_0 - \mathbf{h}_0^*; \\ \frac{d\Delta}{dt} = W_h \Delta; \end{cases}$$

Solution: $\Delta(t) : [0, T] \rightarrow \mathbb{R}^d$.

This equation can be solved in closed form, via the well-known theory for matrix ODEs, in terms of the eigenvalues λ_i and eigenvectors \mathbf{v}_i of W_h :

$$\Delta(t) = \sum_i C_i \mathbf{v}_i e^{\lambda_i t},$$

for some constants C_i , which are currently none of our concern. The equation (19) follows directly from this expression. □

B DATA PREPROCESSING

Data preprocessing is an important aspect in addition to the main part. Below are two datasets with specific features.

WISDM. Due to the large size of these sequences, we split them into 15-second windows, classifying each such window separately. A 20Hz observation frequency leaves us with 300 observations per window. Note that this is not an irregular sequence dataset in the true sense since the observations are actually uniformly distributed and correspond to a continuous process. Nevertheless, we find it interesting to test our models in this scenario as well since it is consistent with our reasoning behind the proposed methods.

Retail. We preprocessed the product descriptions via TF-IDF and extracted top-125 components using a truncated SVD decomposition. Combining them with quantity, price, and time since the last purchase leaves us with 128 features. We posed the task of classifying of the customer's countries of origin. This dataset has a significant class imbalance, with 90% customers from the United Kingdom (UK). To combat this imbalance, we settled on one-vs-all binary labels indicating whether the customer is from the UK.

C KERNEL SCALE ABLATION

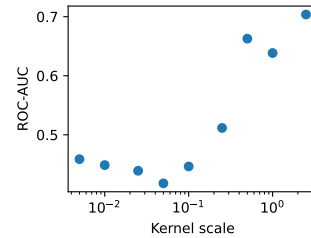


Figure 5: The relationship between the kernel scale γ (x-axis, log-scale) and the resulting ROC-AUC metric (y-axis).

Apart from varying interpolation regimes and negative feedback, we also tried changing the kernel scale γ :

$$K(\tau) = e^{-\gamma^2 \tau^2}.$$

The results for the HSBC dataset are presented in Figure 5. As can be seen, smaller values of γ cause decreases in quality. On the other hand, larger values caused greater numerical instability, as they

lead to degenerate covariance matrices [8]. We conclude that the default value of $\gamma = 1$ provides a reasonable compromise, which worked reasonably on all datasets.